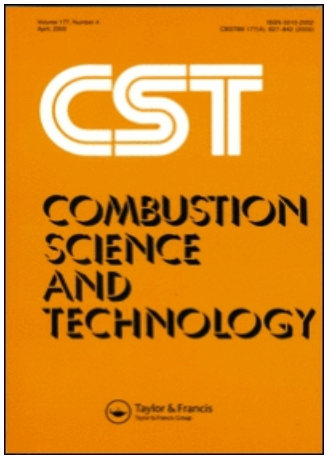

Combustion Science and Technology
Publication details, including instructions for authors and subscription information:
http://www.informaworld.com/smpp/title~content=t713456315

Flow Studies in Non Circular Tubes with Wall Injection

H. S. Mukunda [a]; A. Subhananda [a]; M. Sambashiva Rao [a]
[a] Department of Aeronautical Engeering, Indian Institute of Science, Bangalore, India

Online Publication Date: 01 January 1977
To cite this Article: Mukunda, H. S., Subhananda, A. and Rao, M. Sambashiva (1977) 'Flow Studies in Non Circular Tubes with Wall Injection', Combustion Science and Technology, 15:1, 21 - 30
To link to this article: DOI: 10.1080/00102207708946767
URL: http://dx.doi.org/10.1080/00102207708946767

Combustion Science and Technology
1977, Vol. 15, pp. 21–30

Flow Studies in Non Circular Tubes with Wall Injection

H. S. MUKUNDA, A. SUBHANANDA RAO and M. SAMBASHIVA RAO *Department of Aeronautical Engineering, Indian Institute of Science, Bangalore 560012, India*

(Received October 8, 1975; in final form January 22, 1976)

Abstract—An analysis of inviscid incompressible flow in a tube of sinusoidally perturbed circular cross section with wall injection has been made. The velocity and pressure fields have been obtained. Measurements of axial velocity profiles and pressure distribution have been made in a simulated star shaped tube with wall injection. The static pressure at the star recess is found to be more than that at the star point, this feature being in conformity with the analytical result. Flow visualisation by photography of injected smoke seems to show simple diffusion rather than strong vortices in the recess.

1 INTRODUCTION

Noncircular shapes like star and wagon wheel have been used as the cross section for internally burning grains rather extensively in solid propellant rocket motors due to demand for large burning area for limited lengths and diameters of the grain. These configurations, in addition, have the flexibility of having any of the progressive, neutral, and/or regressive nature of burning. In order to study the erosive phenomenon in these grains, it is necessary to have an understanding of the flow structure in noncircular tubes with mass injection at the wall normal to the surface. Culick (1966) presented an analytical solution for the flow of inviscid incompressible flow in a cylindrical duct with wall injection. Subsequent to this, no analytical studies seem to have been made on noncircular ducts. The present paper attempts at analysing the three dimensional flow structure in a slightly perturbed circular duct with wall injection. In cases where wall mass injection is reasonably large compared to main stream flow, it is a good approximation to treat the flow as inviscid as blowing through the wall reduces the viscous effects in the field. The flow situation in the port of a rocket propellant grain is generally subsonic, except where strong erosion is introduced through the use of sections with port area comparable to that of throat area. In any case, the assumption of incompressibility will actually be satisfied over a considerable portion of the grain.

With regard to experimental studies, Dunlop *et al.* (1974) seem to be the only workers who have measured the velocity profiles inside a circular duct with wall injection. They have measured the velocity profiles using a hot-wire anemometer and the results confirm the analytical results of Culick (1966).

In the present paper, analytical studies are presented first, experiments described next and these are together discussed subsequently.

2 GOVERNING EQUATIONS

Figure 1a shows the approximation of the actual star-shaped grain by a perturbed star configuration. Figure 1b shows the coordinate system chosen. The amplitude of the perturbation of the wall given by $\epsilon = 1 - r_w/a$ is taken small. The basic equations of flow for the present case are Euler's equations of motion. They are

$$\frac{\partial v_r}{\partial r} + \frac{1}{r}\frac{\partial v_\theta}{\partial \theta} + \frac{\partial v_z}{\partial z} + \frac{v_r}{r} = 0 \tag{1}$$

$$v_r\frac{\partial v_r}{\partial r} + \frac{v_\theta}{r}\frac{\partial v_r}{\partial \theta} + v_z\frac{\partial v_r}{\partial z} - \frac{v_\theta^2}{r} = -\frac{1}{\rho}\frac{\partial p}{\partial r} \tag{2}$$

$$v_r\frac{\partial v_\theta}{\partial r} + \frac{v_\theta}{r}\frac{\partial v_\theta}{\partial \theta} + v_z\frac{\partial v_\theta}{\partial z} + \frac{v_r v_\theta}{r} = -\frac{1}{\rho}\frac{1}{r}\frac{\partial p}{\partial \theta} \tag{3}$$

$$v_r\frac{\partial v_z}{\partial r} + \frac{v_\theta}{r}\frac{\partial v_z}{\partial \theta} + v_z\frac{\partial v_z}{\partial z} = -\frac{1}{\rho}\frac{\partial p}{\partial z} \tag{4}$$

$$\rho = \text{constant} \tag{5}$$

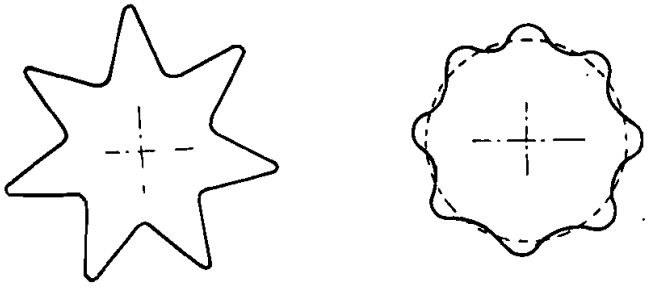

(a)

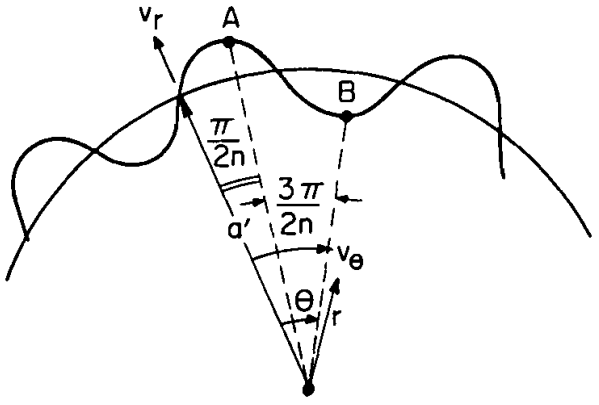

r_w = Radius of the wall
rw = a'(1 + ϵ sin nθ)
n = No. of stars
A = Star recess (nθ = $\pi/2$)
B = Star point (nθ = $3\pi/2$)
z = Coordinate in axial direction
v_z = Velocity in z-direction

(b)

FIGURE 1 (a) Schematic of the grain shape; (b) the coordinate system.

where r, z are the radial and axial coordinates already nondimensionalised with the mean radius a'. The boundary conditions are,

$$\text{at } r = r_w,\ v_z = 0,\ \text{normal velocity } v_n = -v_w$$
$$\text{at } r = 0,\quad v_r = 0. \tag{6}$$

Since the flow configuration is three dimensional, two stream functions are needed to describe the flow. The stream functions ϕ and ψ are defined by

$$v_z = \frac{1}{r}\frac{\partial \phi}{\partial r},\quad v_\theta = \frac{\partial \psi}{\partial r}$$
$$v_r = -\frac{1}{r}\left[\frac{\partial \psi}{\partial \theta} + \frac{\partial \phi}{\partial z}\right] \tag{7}$$

such that the equation of mass conservation (1) is satisfied by these relations.

The solutions for ϕ and ψ are obtained as a perturbation series as

$$\phi = \phi_0 + \epsilon\phi_1 + 0(\epsilon^2)$$
$$\psi = \psi_0 + \epsilon\psi_1 + 0(\epsilon^2)$$
$$p = p_0 + \epsilon p_1 + 0(\epsilon^2) \tag{8}$$

It may be noted that ϕ_0 constitutes the solution for the circular geometry as obtained by Culick (1966). This solution along with that for ψ_0 and p_0 can be written as

$$\phi_0 = v_w z \sin\frac{\pi r^2}{2}$$
$$\psi_0 = 0$$
$$p_0 = P^0 - \frac{\rho v_w^2}{2}\left[\frac{\sin^2(\pi r^2/2)}{r^2} + \pi^2 z^2\right] \tag{9}$$

where P^0 is the stagnation pressure determined at $(r, z, \theta) = (0, 0, 0)$.

Substitution of Eqs. (7) and (8) in Eqs. (2–4) leads to the following equations for order ϵ.

$$\frac{\partial}{\partial r}\left\{p_1 + \frac{\rho v_w}{r^2}\sin\frac{\pi r^2}{2}\left(\frac{\partial\phi_1}{\partial z} + \frac{\partial\psi_1}{\partial\theta}\right)\right\} - \frac{\rho v_w}{r}\pi z\cos\frac{\pi r^2}{2}\left(\frac{\partial^2\psi_1}{\partial\theta\partial z} + \frac{\partial^2\phi_1}{\partial z^2}\right) = 0$$

$$\rho v_w \sin\frac{\pi r^2}{2}\left\{\frac{\partial^2\psi_1}{\partial r^2} + \frac{1}{r}\frac{\partial\psi_1}{\partial r}\right\} - \rho r v_w z\pi\cos\frac{\pi r^2}{2}\frac{\partial^2\psi_1}{\partial r\partial z} = \frac{\partial P_1}{\partial\theta}$$

$$\frac{\partial}{\partial z}\left\{p_1 + \frac{\rho v_w z}{r}\pi\cos\frac{\pi r^2}{2}\frac{\partial\phi_1}{\partial r}\right\} + \pi^2 v_w z\sin\frac{\pi r^2}{2}\left(\frac{\partial\psi_1}{\partial\theta} + \frac{\partial\phi_1}{\partial z}\right) - \frac{\rho v_w}{r^2}\sin\frac{\pi r^2}{2}\left\{\frac{\partial^2\phi_1}{\partial r^2} - \frac{1}{r}\frac{\partial\phi_1}{\partial r}\right\} = 0$$

On integration and simplification, the above equations will lead to

$$p' - r^2\int_0^\theta\left(\frac{\partial^2\psi_1}{\partial r^2} + \frac{1}{r}\frac{\partial\psi_1}{\partial r}\right)d\theta + \pi r^3 z\cot\frac{\pi r^2}{2}\int_0^\theta\frac{\partial^2\psi_1}{\partial r\partial z}d\theta = F_{31}(z)F_{32}(r) \quad (10)$$

$$p' + \left(\frac{\partial\phi_1}{\partial z} + \frac{\partial\psi_1}{\partial\theta}\right) - \frac{\pi r^2 z}{\sin(\pi r^2/2)}\int_0^r\frac{1}{r}\cos\frac{\pi r^2}{2}\left(\frac{\partial^2\psi_1}{\partial\theta\partial z} + \frac{\partial^2\phi_1}{\partial z^2}\right)dr = \frac{r^2 F_{41}(z)F_{42}(\theta)}{(\rho v)_w\sin(\pi r^2/2)} \quad (11)$$

$$p' + \pi r z\cos\frac{\pi r^2}{2}\frac{\partial\phi_1}{\partial r} + \pi^2 r^2\int_0^z z\left(\frac{\partial\phi_1}{\partial z} + \frac{\partial\psi_1}{\partial\theta}\right)dz - \int_0^z\left(\frac{\partial^2\phi_1}{\partial r^2} - \frac{1}{r}\frac{\partial\phi_1}{\partial r}\right)dz = F_{51}(r)F_{52}(\theta) \quad (12)$$

where

$$p' = \frac{p_1 r^2}{(\rho v)_w\sin(\pi r^2/2)} \quad (13)$$

The integration functions on the right-hand side have all been deliberately chosen in a variable separable form in view of the fact that solutions in variable separable form will be sought. Substitution of the forms

$$\psi_1 = R_1(r)T_1(\theta)Z_1(z);$$
$$\phi_1 = R_2(r)T_2(\theta)Z_2(z) \quad (14)$$

into the Eqs. (10–12) leads to

$$p' - r^2\left(R_1'' + \frac{R_1'}{r}\right)Z_1\int_0^\theta T_1\,d\theta + \pi r^3\cot\frac{\pi r^2}{2} \times R_1' z Z_1'\int_0^\theta T_1\,d\theta = F_{31}(z)F_{32}(r) \quad (15)$$

$$p' + R_2 Z_2' T_2 + R_1 Z_1 T_1' - \frac{\pi r^2}{\sin(\pi r^2/2)}\int_0^r\frac{\cos(\pi r^2/2)}{r}R_2\,dr\,zZ_2''T_2 - \frac{\pi r^2}{\sin(\pi r^2/2)}\int_0^r\frac{\cos(\pi r^2/2)}{r}R_1\,dr\,zZ_1'T_1' = \frac{r^2 F_{41}(z)F_{42}(\theta)}{(\rho v)_w\sin(\pi r^2/2)} \quad (16)$$

$$p' + \pi r \cot\frac{\pi r^2}{2} R_2' z Z_2' T_2 + \pi^2 r^2 R_2 \int_0^z z Z_2' dz\, T_2$$

$$+ \pi^2 r^2 R_1 \int_0^z z Z_1 dz\, T_1' - \left(R_2'' - \frac{R_2'}{r}\right) \int_0^z Z_2 dz\, T_2$$

$$= F_{51}(r) F_{52}(\theta) \qquad (17)$$

The above three integrals must be consistent in order to maintain the separability of the solution. This is possible if and only if $Z_1 = 1$ and $Z_2 = z$. It follows then that $T_1 = \cos(n\theta)$ and $T_2 = \sin(n\theta)$. Further comparison leads to

$$r^2 R_1'' + r R_1' - n^2 R_1 + n R_2 = 0 \qquad (18)$$

$$r^2 R_2'' - r R_2' \left(2\pi r^2 \cot\frac{\pi r^2}{2} + 1\right)$$

$$- \pi^2 r^4 R_2 + n\pi^2 r^4 R_1 = 0 \qquad (19)$$

and

$$F_{31}(z) = F_{41}(z) = 0$$

$$F_{51}(r) = (r^2 R_1'' + r R_1');$$

$$F_{52}(\theta) = \sin(n\theta)/n \qquad (20)$$

Thus the problem reduces to the solution of the Eqs. (18) and (19) subject to the following boundary conditions:

$$\text{at } r = 1; \quad R_2' = \pi^2 v_w; \quad R_2 - n R_1 = -v_w$$

$$\text{at } r = 0; \quad R_1 = R_2 = 0. \qquad (21)$$

These boundary conditions are obtained from Eqs. (5) and (6) as demonstrated in the Appendix.

Equations (18) and (19) are ordinary differential equations with variable coefficients. The point $r = 0$ constitutes a regular singular point for both the equations. It is also to be noted that the range of r is small (~ 1). Hence a series solution may be obtained by using the Frobenius technique. The solutions for $n = 5$ are

$$R_1 = 2.295 v_w r^5 (1 - 0.836r + 0.152r^4 - 0.040r^7)$$

$$R_2 = 4.309 v_w r^6 (1 - 0.985r^3 + 0.318r^4 - 0.154r^7) \qquad (22)$$

The solutions for $n = 3$ and 4 have been discussed by Subhananda Rao (1975). One now obtains the velocity and pressure distribution as

$$\frac{v_z}{v_w} = \pi z \sin\frac{\pi r^2}{2} + 25.855\epsilon r^4 (1 - 1.478r^3$$

$$+ 0.530r^4 + 0.358r^5) z \sin 5\theta$$

$$\frac{v}{v_w} = 11.475\epsilon r^4 (1 - 1.003r$$

$$+ 0.294r^4 - 0.079r^5) \cos 5\theta$$

$$\frac{v_r}{v_w} = -\frac{1}{r} \sin\frac{\pi r^2}{2} + 11.475\epsilon r^4 [1 - 1.211r$$

$$+ 0.522r^4 - 0.159r^9 - 0.058r^{12}]$$

$$p = p^0 - \frac{\rho v_w^2}{2}\left[\frac{1}{r^2}\sin\frac{\pi r^2}{2} + \pi z^2\right]$$

$$+ \epsilon\left(R_1'' + \frac{R_1'}{r}\right) v_w \sin\frac{\pi r^2}{2} (\sin 5\theta)/5$$

The analytical results using the above equations are presented subsequently along with the experimental results.

3 THE EXPERIMENTS

The experimental set-up used for the present investigation is shown in Figure 1 and Plate 1. The apparatus consists of a porous brass tube made into a six-star configuration to simulate the propellant surface. Three glass tubes separated by perspex spacers enclose the brass tube. One end of this is closed and a nozzle is fixed to the other end. The nozzle is used so as to obtain the required back pressure. Air enters through the passages in the spacers into the annular space between the brass tube and the glass tube. The air enters afterwards through the pores in the brass tube and flows axially through the port. Typical velocities in the annular space are about 8–10 cm/sec whereas the axial velocity in the brass tube is about 150 cm/sec in the head end bay and about 450 cm/sec in the bay towards the nozzle end. The flow entering the apparatus is monitored by a rotameter.

In order to determine the possible static pressure difference between the star point and the star recess, radial tappings are made at three axial stations and

the difference between the pressures is measured using a projection manometer. The details of this part are shown in Figure 2. Axial velocities at various radial locations are obtained by measuring the stagnation and static pressures. The stagnation pressure probe is a hypodermic needle of 1 mm outer dia. and 0.5 mm inner dia. with one end connected to the projection manometer. The static pressure probe is also a hypodermic needle of the same dimensions with front end closed and a hole of 0.5 mm on the side wall.

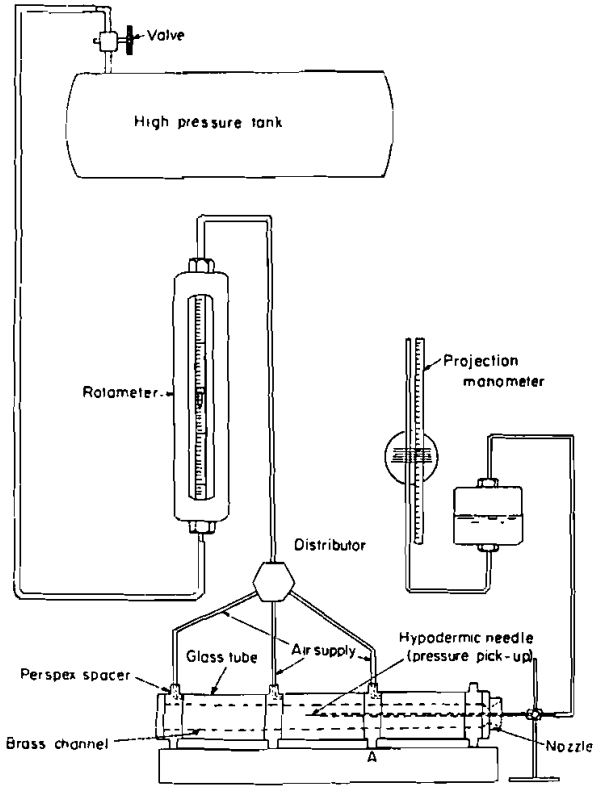

FIGURE 2 Schematic of the experimental set-up.

The flow rate is varied between 50 and 150 lit/min. Velocity distribution on the axis and also radially in the star and recess planes is determined.

4 RESULTS AND DISCUSSION

The results of the experiments as well as analysis are presented in Figures 4–10. It must be emphasised that the experimental results pertain to a six-point star configuration, whereas the analytical

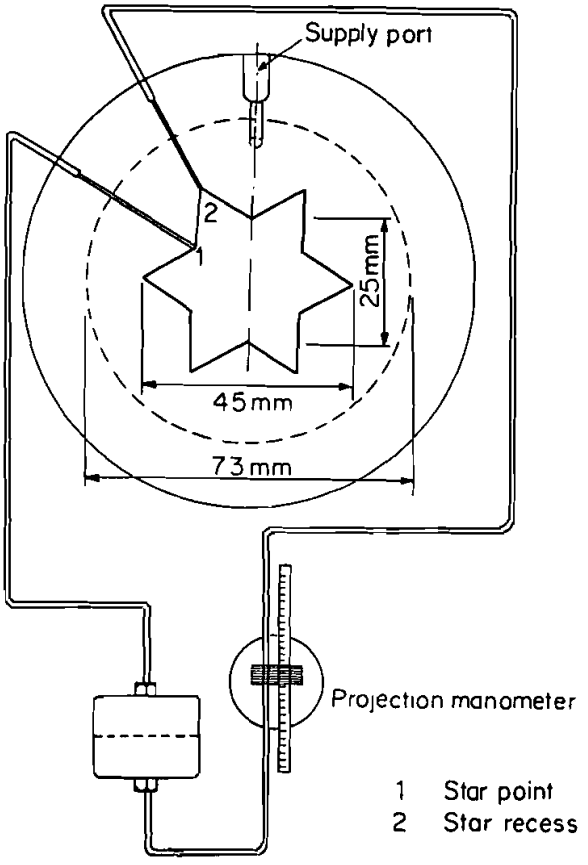

FIGURE 3 Details at Section A.

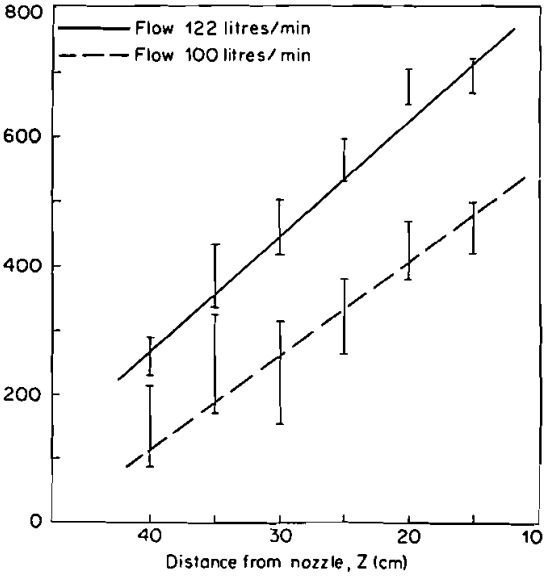

FIGURE 4 Centre-line velocity.

results refer to a weakly perturbed circular tube of five stars with $\epsilon = 0.1$. The Comparison between the two sets of results can be expected *only in the qualitative sense.*

Figure 4 shows the plot of centre line axial velocity with axial distance as obtained experimentally. The results seem to indicate a linear variation with distance. The accuracy of the experimental result has been rather poor because the resolution of the projection manometer was rather poor (0.25 mm in 2.5–4 mm). The analytical result predicts a variation of v_z at the central line to the first approximation to be linear in z. It is likely this characteristic of linear variation of $v_z(0, z, 0)$ with z is not dependent on the strength of perturbation (ϵ being large). Figure 5 shows the plot of the radial velocity *vs.* radius as obtained from analysis. It

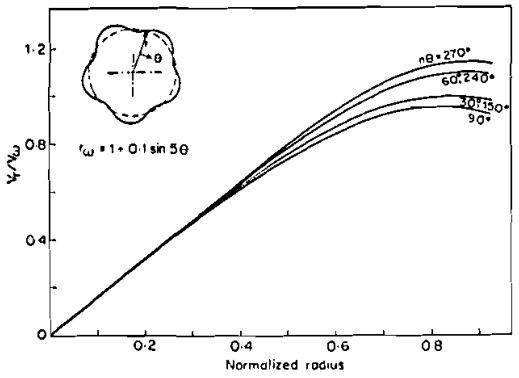

FIGURE 5 Plot of v_r versus r at different angular positions.

appears that the radial velocity exceeds the wall injection velocity near the wall by about 20 percent. Figure 6 contains the measured axial velocity variation across the radius. It appears that velocity along a star recess (along B) is larger than along the star point plane (along B) up to some radius (of 6.0 mm here). This appears to be true even though there is reasonable scatter in the experiments. Around 6.5 mm on either side, the velocity starts increasing along section A whereas along B the velocity continues decreasing. This feature was confirmed in several experiments. The larger velocity along section B in comparison with that along A is confirmed in the analytical results. These are plotted in Figure 7. The velocity variation along $n\theta = 90°$ (recess) is more than that along $n\theta = 270°$ (point). The theoretical prediction is that the axial velocity continuously decreases from star recess plane to star point plane.

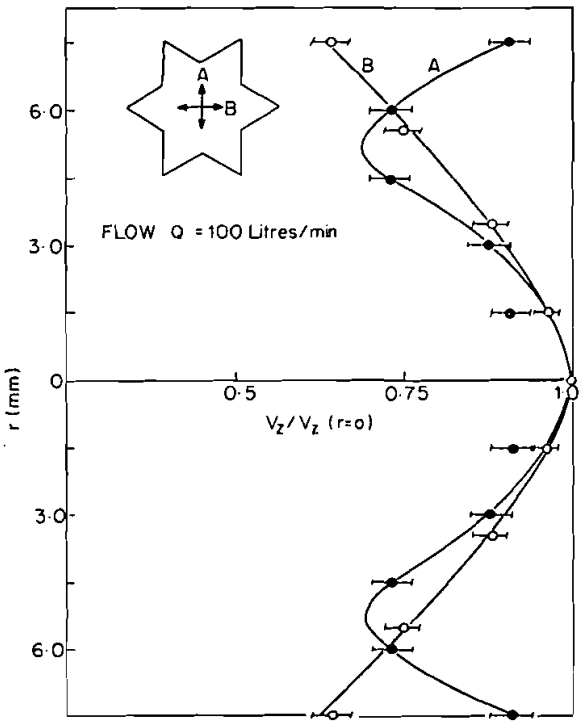

FIGURE 6 Normalized velocity variation in star point and star recess planes (15 cm from nozzle).

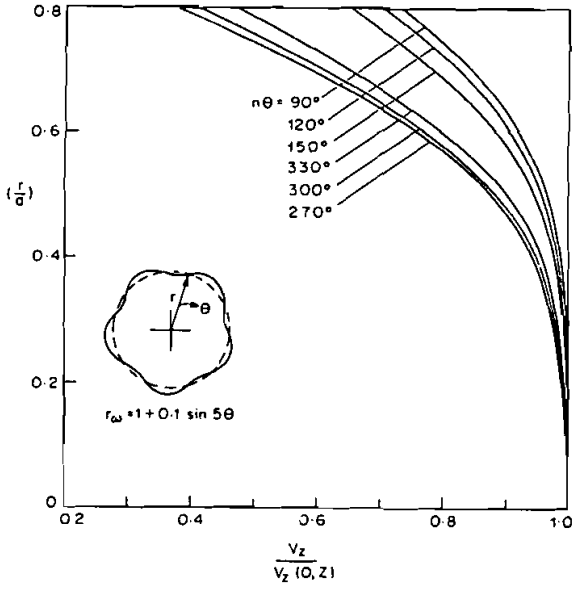

FIGURE 7 Plot of velocity in z direction (v_z) versus r at different angular positions.

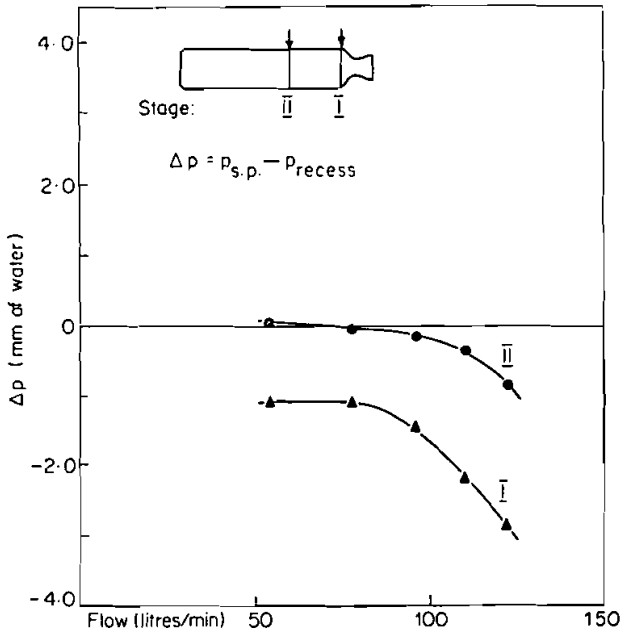

FIGURE 8 Pressure difference at star point and star recess with flow.

The deep shift in velocity profiles along A as observed in Figure 6 may be obtained from an analysis of the flow in the star, a feature that probably is not obtainable in flow through a perturbed tube.

The results of static pressure difference between star point and recess are shown in Figures 8 and 9. The theoretical prediction is that the star recess has a higher static pressure compared to star point (Figure 9). This feature is confirmed in the experiments also. The behaviour of the Δp at stations I and II show the trend expected in the analysis (Figure 8).

Figure 10 shows the tangential velocity variation with radius. The tangential velocity builds up towards the wall and is about 20–25 percent of the injection velocity. In order to find if this level of tangential velocity results in strong vortices which can be observed by flow visualisation techniques, a flow visualisation experiment was conducted. Smoke generated from a standard (kerosene + turpentine) smoke generator was used to inject the smoke through the static holes at the star point and the star recess separately. Then the main flow would be put on and the flow examined. With the intention of examining the possible vortex structure at the corner, intense cross lighting with photography along the axis was adopted but not with much success. Subsequently lighting from a corner was used and the flow pictures were taken. These are shown in Plates 2 and 3. These photographs show no significant formation of vortices. In fact these appear to be cases of simple diffusion. It must be brought out that the axial velocities

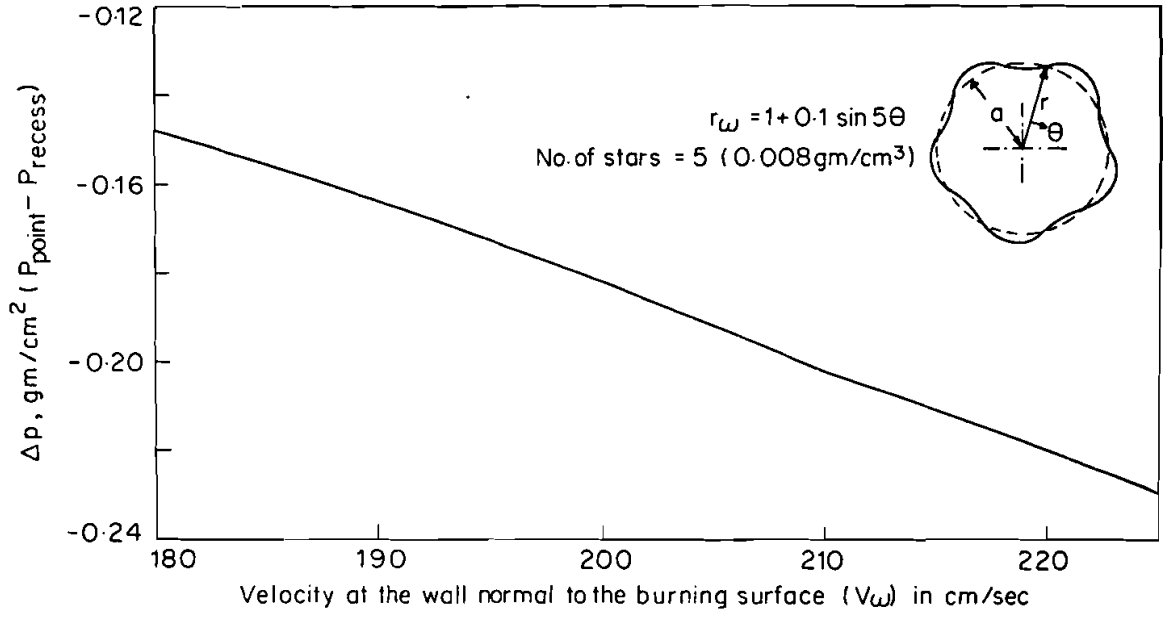

FIGURE 9 Plot of static pressure difference between star point and recess versus v_w.

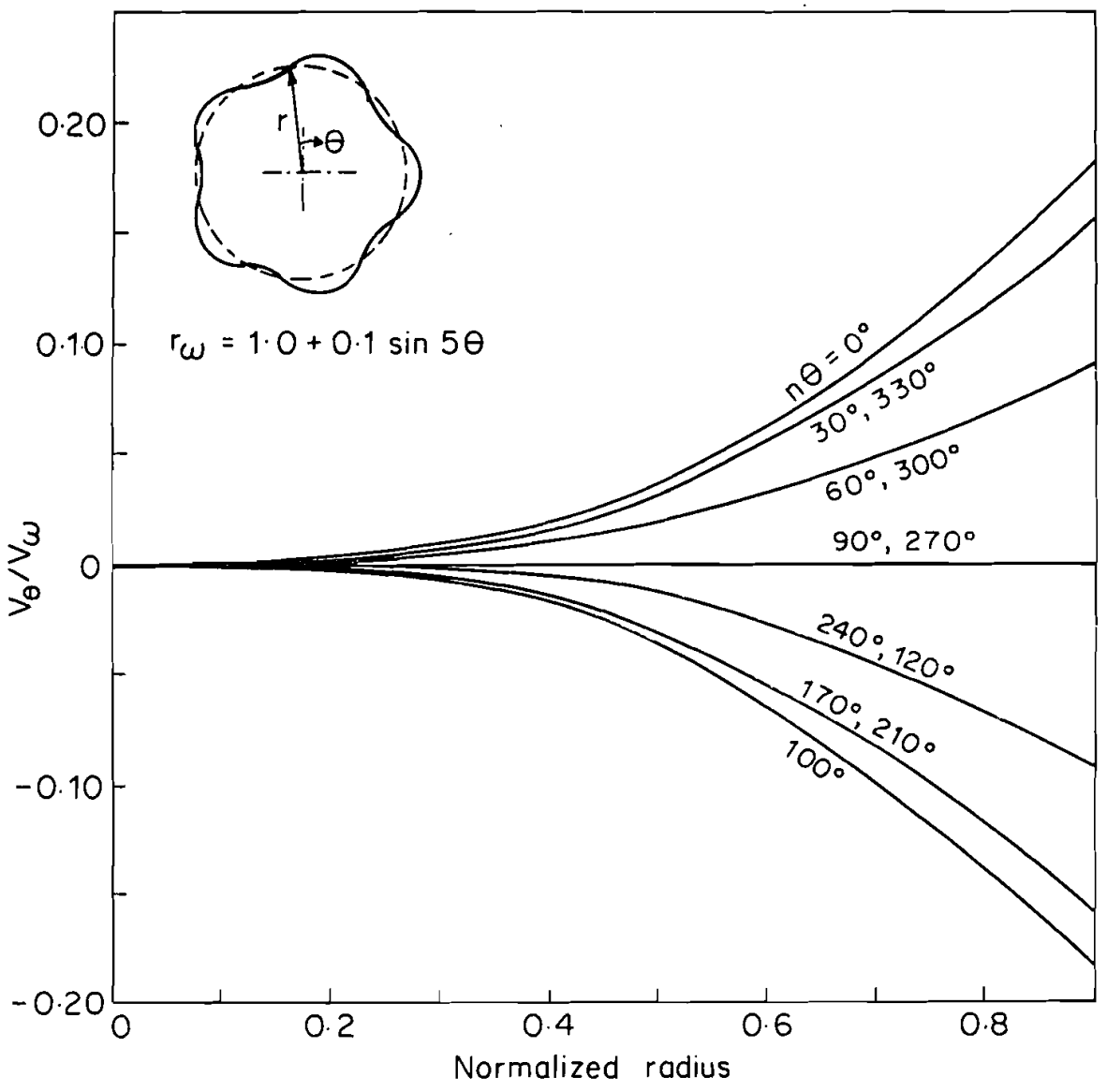

FIGURE 10 Plot of velocity in θ direction (v_θ) versus r at different angular positions.

were quite low (50 cm/sec) when these photographs were taken. Higher speeds would cause intense mixing at the recess itself thus preventing flow visualisation. As such, it is not clear if higher speeds do not lead to formation of vortices.

A few remarks of relevance to erosive burning applications are in order. In a noncircular cross section, the burning rates at various positions in the cross sections are unlikely to be the same. The burning rate is quite strongly dependent on pressure under erosive/nonerosive conditions. It is noticed from the above investigation that the star recess is likely to experience higher burning rate in comparison to star point if pressure were the sole parameter determining the burning rate. However, experimental observations (Williams *et al.*, 1969) show that regression rates are higher near star point in comparison to star recess. The anomaly may be due to the fact that the hot flow conditions (both in experiments as well as analysis) produce a different pressure distribution in comparison to cold flow conditions. This point needs to be clarified through more investigation.

5 CONCLUSIONS

The analytical and experimental results lead to the following conclusions:

1) Static pressure is higher at the star recess compared to the star point.

2) Axial velocities in the star recess plane are larger than in the star point plane.

3) Axial velocity seems to vary linearly along the central axis.

4) The tangential velocity is about 20–25 percent of the injection velocity.

5) Vortex strength is too small to be observed in the flow visualisation experiments.

ACKNOWLEDGEMENTS

Thanks are due to Mr. B. N. Raghunandan for helpful criticism on the manuscript. A. Subhananda Rao and M. Sambashiva Rao are now at D.R.D.L. Hyderabad.

REFERENCES

Culick, F. E. C. (1966). Rotational axisymmetric mean flow and damping of acoustic waves in solid propellant rockets, *AIAA Journal*, **4**, 1462.

Dunlop, R., Willoughby, P. G., and Hermson, R. W. (1974). Flow field in the combustion chamber of a solid propellant rocket motor. *AIAA Journal*, **12**, 1440.

Subhananda Rao, A. (1975). Studies on erosive burning in star configurations. M.E. Dissertation, Dept. of Aero. Engg., Indian Institute of Science, Bangalore.

Williams, F. A., Barrere, M., and Huang, N. C. (1969). Fundamental aspects of solid propellant rockets. AGARDograph 116, Technivision Services Slough, England.

Appendix

The boundary conditions:

1) At the boundary, $r = 1 + \epsilon \sin n\theta$, $v_z = 0$.

$$v_z = \frac{1}{r}\frac{\partial \phi}{\partial r} = \frac{1}{r}\left[\pi v_w r z \cos\frac{\pi r^2}{2} + \epsilon R_2' z \sin n\theta\right]$$

$$v_{z_{r=r_w}} = \pi v_w z \cos\left[\frac{\pi}{2}(1+\epsilon \sin n\theta)^2\right] + \frac{\epsilon R_2'(1) z \sin n\theta}{1+\epsilon \sin n\theta}$$

On making Taylor series expansion and retaining terms of $0(\epsilon)$ we get,

$$R_2'(1) = \pi^2 v_w.$$

2) Similarly the condition that normal velocity$\}_{\text{wall}} = -v_w$ leads to $R_2 - nR_1 = -v_w$.

3) At $r = 0$, one obtains $R_1 = R_2 = 0$.